IPN Progress Report 42-184 • February 15, 2011

Optical Phase Lock Loop Based Phased Array Transmitter for Optical Communications

Yasha Vilenchik*, Baris I. Erkmen†, Naresh Satyan‡, Amnon Yariv*‡, William H. Farr†, and John M. Choi†

We propose a novel deep space optical communication scheme, in which an integrated optical phased array (OPA) is used for both phase modulation and fine beam steering. In particular, an optical phase-locked loop (OPLL) based phased array with full electronic control over the phase is introduced and analyzed. The performance of such an array as a beam steering mechanism is evaluated and compared to realistic steering requirements for deep space applications. It is shown that an array with a high fill factor (> 0.7) with about 300 elements per dimension is needed to meet these requirements. The effect of residual phase noise due to limited loop bandwidth is analyzed. Finally the theory is validated by experimental results demonstrating successful beam steering using a two element phased array.

I. Introduction

The science returns from virtually all missions, near-Earth and deep space alike, are limited by the communication downlink rate to Earth, which are, in turn, limited by power and spectrum allocation. Optical communications has emerged as a solution offering order-of-magnitude increases in data rate and available modulation spectrum. The current deep-space optical communications paradigm relies on sending high peak power laser pulses with a low duty cycle, such that a low average power is maintained. Typical lasers in this category have low wall-plug-to-output power conversion efficiency (e.g. < 25 % with state-of-the-art fiber lasers). The need for accurate pointing of both the transmitter and receiver nodes is typically achieved with mechanical fine-steering, i.e., by using

*Department of Applied Physics, California Institute of Technology

†Communications Architectures Research Section

‡Department of Electrical Engineering, California Institute of Technology

The research described in this publication were carried out by the Jet Propulsion Laboratory, California Institute of Technology, under a contract with the National Aeronautics and Space Administration.

high-bandwidth, feedback-controlled tip and tilt mirrors or piezo-electric actuators. This steering mechanism is a critical component of the spacecraft transmitter optics, and therefore it constitutes a single-point failure to the communication link.

One possible paradigm shift that addresses both the issue of low efficiency and the need of mechanical fine steering mechanism, is the use of an optical phased array transmitter. The precise phase control mechanism of these transmitters renders them inherently suitable for phase modulation, which in turn facilitates the use of high-wallplug-efficiency (~ 70 %) continuous-wave (CW) lasers. Moreover, just like radio frequency (RF) phased-array antennas, beam steering through wave front control is easily achieved without relying on mechanical fine-steering. In addition, due to the large redundancy offered by the many laser-emitting elements, the performance of the array degrades only marginally if a few of the array elements malfunction. If phase-modulated optical communications technology employing optical phased array transmitters can be coupled with quantum-limited advanced optical phase-sensitive receivers, then a new communication paradigm emerges, one with significantly less power consumption and physical size and weight than those required by the state-of-the-art optical communications transmitters.

Phased array antennas have had significant success in the RF domain for beam forming, steering, communication and 3D imaging applications. Analogous efforts and advances in the optical domain however, have had limited success. Past demonstrations of phased array beam steering have required injection locking of the individual laser elements in the array [1], which is inherently unstable and difficult to scale due to complexity and cost. An alternative method utilizing a single laser, which is expanded and passed through an array of phase modulators, has resulted in limited output power [2]. Furthermore, the state-of-the-art for this method utilizes liquid crystal spatial light modulators, which have limited bandwidth, and are not very well suited for operation in the space environment.

An alternative emerging technology for optical phased arrays that overcomes the fundamental challenges encountered by previous approaches is enabled using fully electronically controllable optical phase-locked loops (OPLLs). Members of our team at the California Institute of Technology have recently demonstrated preliminary success in coherent combination of multiple independent lasers, using OPLLs [3, 4]. This method constitutes the crux of our novel phased-array transmitter concept, which is illustrated in Figure 1. An array of semiconductor lasers is locked to a common master laser using heterodyne OPLLs. Electronic phase shifters are utilized to control the phase of the offset signal to each OPLL, hence controlling the phase of each individual laser emitter. Fast and robust steering is accomplished by imparting a time-varying linear phase profile to the electronic phase shifters.

II. Optical Phased Array - Theory

In this article we shall limit our treatment to the one-dimensional array shown in Figure 2, as this is sufficient to characterize the experimental demonstration that we report in the

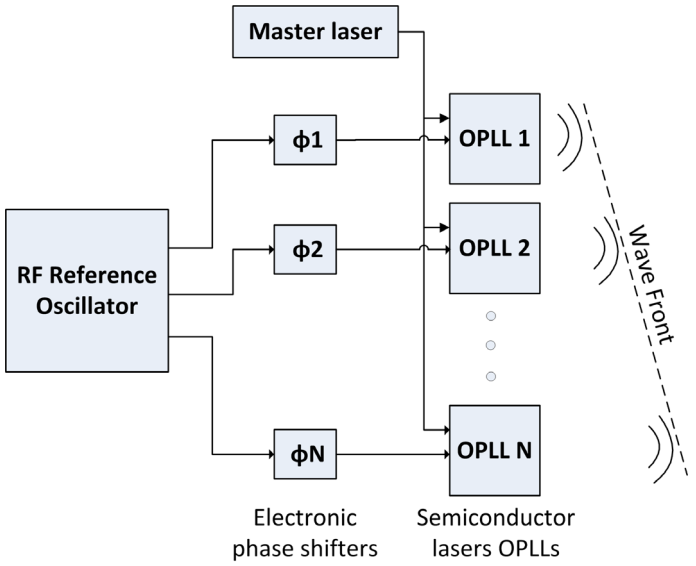

Figure 1. A block diagram representation of the novel optical phased array implementation concept. An array of semiconductor lasers is locked to a master laser. The phase of each laser in the array is controlled electronically.

subsequent section. Consider a paraxial, z-directed beam propagation geometry, where all optical source emitters are placed on the $z = 0$ plane. Suppose that a total of $(2M + 1)$ emitters ($M \in \mathbb{Z}$), each with diameter d_a, are spaced equally apart by d_s along the x axis on this plane, with the center element of the array aligned with the optical axis. We assume that each laser element emits a monochromatic, scalar and paraxial beam with center-wavelength λ_0. The baseband envelope of the n-th element, with units normalized to $\sqrt{\text{Watts/m}^2}$, is given by

$$E_n(x, y, 0) = \sqrt{\frac{P_n}{A}} e^{in\Delta\phi}\, W\left(\frac{x - nd_s}{d_a}, \frac{y}{d_a}\right), \tag{1}$$

at the transverse coordinate (x, y) on the $z = 0$ plane. Here $n = -M, \ldots, M$, $W(x, y)$ describes the identical axial beam profile that is exiting each emitter aperture, $A \equiv d_a^2 \int W^2(x, y)\mathrm{d}x\mathrm{d}y$, P_n is the power output of the n^{th} emitter, and $\Delta\phi$ is the linear phase increment in each emitter. The 'Fill Factor' is defined as $\gamma = \frac{d_a}{d_s}$, and is a measure of the effective relative area of the array that is actually filled with light.

When the far field propagation condition $L \gg \pi d_a^2/\lambda_0$ prevails, the intensity of the field on the $z = L$ plane is given by using the Fraunhofer far field approximation

$$I(x, y, L) \equiv |E(x, y, L)|^2 = \frac{P_0 d_a^4}{\lambda_0^2 L^2 A} \left|\mathcal{W}\left(\frac{2\pi d_a}{\lambda_0 L}x, \frac{2\pi d_a}{\lambda_0 L}y\right)\right|^2 \left|\mathcal{E}\left(\frac{2\pi d_s}{\lambda_0 L}x - \Delta\phi\right)\right|^2. \tag{2}$$

where $\mathcal{W}(k_x, k_y) \equiv \int W(x, y)e^{-i(k_x x + k_y y)}\mathrm{d}x\mathrm{d}y$ is the 2D Fourier transform of the beam profile for the individual emitters, and $\mathcal{E}(\Omega) \equiv \sum_{n=-M}^{M} \sqrt{P_n}/\sqrt{P_0}e^{-i\Omega n}$ is the discrete-time

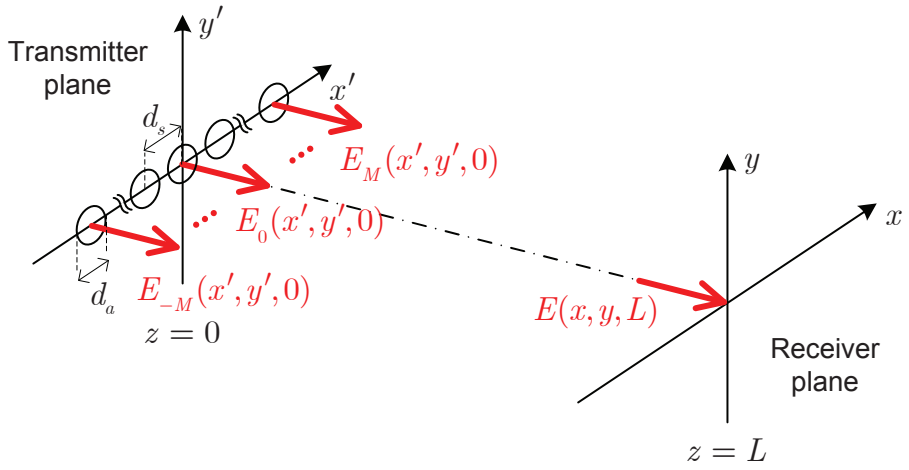

Figure 2. The one dimensional optical phased array paraxial propagation geometry. The fill factor γ is defined as $\frac{d_a}{d_s}$.

Fourier transform of the average field amplitudes from each laser. Several important conclusions can be derived from this generic expression for the far-field irradiance:

- The steerable beam is given by the last term $\mathcal{E}$, which has a main lobe centered at the transverse coordinate
$$x = \frac{\Delta\phi\lambda_0 L}{2\pi d_s} \tag{3}$$
and has a beam width of $\lambda_0 L/(d_s(2M+1))$. Hence, the beam can be steered by varying the parameter $\Delta\phi$.

- The Fourier transform of the beam profile of the individual lasers, $\mathcal{W}$, defines a broad envelope of width proportional to $\lambda_0 L/d_a$, inside which the beam can be steered.

- Since $\mathcal{E}$ is a discrete-time Fourier transform, the beam pattern is periodic with $\lambda_0 L/d_s$, i.e., the same beam pattern repeats along the x axis on the $z = L$ plane with this period.

- The envelope, $\mathcal{W}$, suppresses the spurious periodic replicas relative to the main lobe. However, because $d_a < d_s$, at least one side lobe on each side of the main lobe will be observed. Larger suppression of these side lobes results in more power being concentrated in the main lobe.

- As the beam is steered further away from the optical axis, the side lobe suppression ratio is reduced. For example, if $\Delta\phi = \pi$, the main lobe and side lobe peak irradiances are equal, resulting in half of the transmitted power being diverted in the opposite transverse direction, as can be seen in Figure 3. Consequently, the effective steering angle for the optical phased array is smaller than the envelope width, and the desire for high side lobe suppression must be balanced with the effective steering angle.

To make the rest of our analysis more concrete, let us assume that our laser beam profiles are Gaussian, with $1/e^2$ intensity diameter d_a, i.e.,

$$W(x,y) = e^{-4(x^2+y^2)}\,, \tag{4}$$

and suppose we have a uniform power distribution across all lasers, i.e., $P_n = P_0$ for $n = -M, \ldots, M$. Using Equation(2), the far field irradiance pattern is given by

$$I(x,y,L) = \frac{P_0 d_a^2 \pi}{2\lambda_0^2 L^2} e^{-\frac{1}{2}\left(\frac{\pi d_a}{\lambda_0 L}\right)^2 (x^2+y^2)} \frac{\sin^2\left(\frac{\pi d_s}{\lambda_0 L}(2M+1)[x - \frac{\Delta\phi\lambda_0 L}{2\pi d_s}]\right)}{\sin^2\left(\frac{\pi d_s}{\lambda_0 L}[x - \frac{\Delta\phi\lambda_0 L}{2\pi d_s}]\right)}\,. \tag{5}$$

The far field irradiance $I(x,0,L)$ is plotted in Figure 3, for different values of $\triangle\phi$.

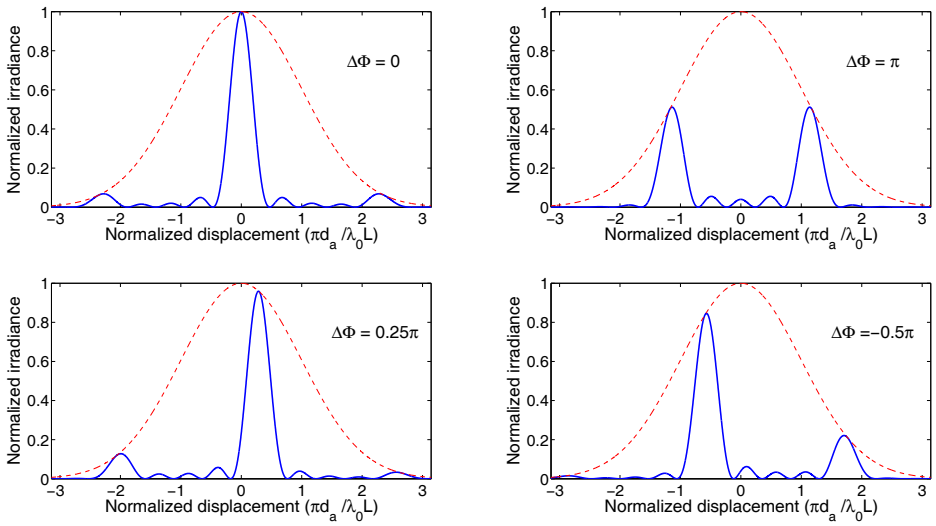

Figure 3. The far-field irradiance pattern of 5 phased-array lasers (M=2) with a Gaussian beam profile and equal power. The dashed curves indicate the envelope defined by the Fourier transform of the Gaussian beam, i.e.,$\mathcal{W}$, and the solid curve is the steered beam. It is evident that as the beam is steered off axis, the main lobe is subject to increasing attenuation, and the side lobe attenuation decreases.

A. Steering angle

From Figure 3, it can be seen that as the beam is steered further away from the optical axis, the power is increasingly diverted from the main lobe to one of the adjacent side lobes, which limits the practical steering range. To quantify this observation, let us assume, with no loss of generality, that $\Delta\phi > 0$. The position of the main lobe, x_m, and the position of its adjacent side lobe, x_s, can be extracted from Equation (5). Let us define the effective steering angle of the optical phased array as the maximal value of $\Delta\phi$ that yields a main lobe peak to side lobe peak irradiance ratio of K ($K \geq 1$), i.e., $\Delta\phi_{max}$ that yields[2]

[2]The ratio of the main lobe and side lobe peak irradiances is a simple parameter that can be used to analytically estimate the fraction of the total energy that is directed in the intended direction.

$$\frac{I(x_m, y, L)}{I(x_s, y, L)} = K\,. \tag{6}$$

Using Equation (5) we find that Equation (6) is satisfied when

$$|\Delta\phi_{max}| = max\left\{0, \pi\left(1 - \frac{2}{\pi^2}\ln(K)\left(\frac{1}{\gamma}\right)^2\right)\right\} \tag{7}$$

Hence, in addition to the suppression factor K, the fill factor γ determines the effective steerable range. We define normalized steering angle as the location of the main lobe, measured in beam width units per emitter - $\frac{1}{(2M+1)}\times$[steerable position in beam width units].

Figure 4 shows the maximum normalized steering angle as a function of the fill factor, for several side lobe suppression values. The suppression factor has logarithmic contribution to the steering range, whereas the fill factor has quadratic dependence. Furthermore, for Gaussian-shaped beam profiles, K cannot exceed $e^{\pi^2/2} \approx 139$.

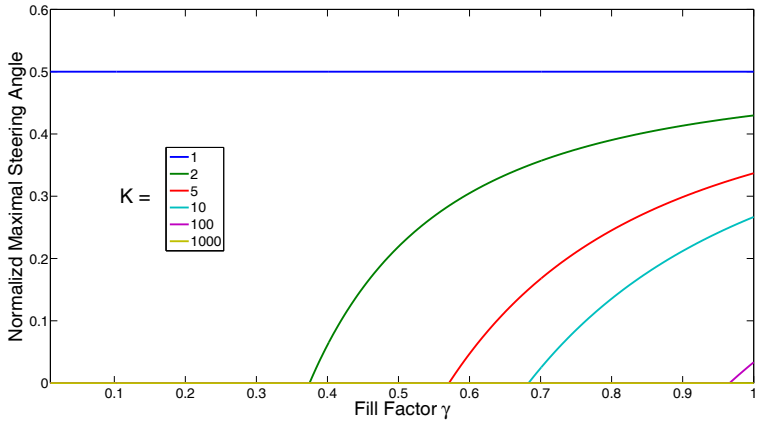

Figure 4. Maximum normalized steering angle ($\frac{1}{(2M+1)}\times$ [maximum steerable position in beam width units]) as a function of fill factor,$\gamma = d_a/d_s$, for several different values of side lobe suppression factor, K.

Note that a fill factor of at least 0.7 is required to achieve steering with a side lobe suppression of 10dB.

B. On-axis irradiance

The capacity of an optical communication link (i.e., the rate of reliable data transfer) is determined primarily by the fraction of transmitted power that couples through the receiver aperture. In a deep-space optical communication link, this quantity is proportional to the far-field on-axis irradiance given by the transmitted beam. The side lobes in an optical phased array imply that a fraction of the transmitted power is not directed to the desired far-field transverse coordinate, which therefore results in a loss factor relative to an optical beam transmitted through a single aperture with the same

dimensions as the phased array. It can be shown from Equation (5) that in order to achieve the same on-axis irradiance with a power-P Gaussian beam of diameter D_G (in the x-axis) and an optical phased array with total power P and fill factor γ, the optical phased array diameter D_{OPA} must satisfy

$$D_{\mathrm{OPA}} = D_G/\gamma\,. \tag{8}$$

It is worthwhile to note from Equations (7) and (8) that the fill factor γ plays a very significant role in determining the steerable range, attainable side lobe suppression and the effective size of the array to deliver comparable power to the far-field. Hence, a high fill factor is critical (for example, $\gamma \geq 0.75$) for high-performance optical phased arrays.

C. OPA for deep space optical communications

Having developed the theoretical limitations of an OPA based steering mechanism, we shall now consider its consequence on deep space communication. Let us consider a deep-space optical communication link from Mars. The maximum point-ahead angle for an optical communication transmitter in Mars orbit is approximately 400 μrad. A diffraction limited 20 cm-diameter transmitter aperture for a 1550 nm center-wavelength downlink beam will yield a beam divergence of approximately 10 μrad, which would result in up to about 40 beam widths of steering to compensate for maximum point-ahead. This represents the approximate range of desired steering capability. The theoretical analysis we have presented in this article demonstrates that the number of beam widths that can be steered (subject to a constraint on the minimum side lobe suppression) is strongly influenced by the fill factor of the phased array, as well as the number of array elements. In particular, we find that if we achieve a reasonable fill factor of 0.80, and require that the side lobes have at least 10 dB suppression relative to the main lobe, a steering range of 40 beam widths requires 300 elements per dimension. In the next section, we analyze a possible realization of an OPA, and discuss its scalability.

III. Realization of an OPA using Optical Phase Lock Loops

Electronic phase-locked loops (PLLs) enable phase synchronization of oscillators, and play a crucial role in today's electronics and communications systems. An optical analog of a PLL has been demonstrated using electronic feedback [5]. One of the more attractive realizations of an optical phase-locked loop (OPLL) can be achieved using semiconductor lasers (SCL). The strong dependence of the SCL's frequency on the injection current, due to the refractive index modulation by free carriers [6], makes it an ideal candidate for OPLLs, where it acts as a current controlled oscillator. Moreover, scalability, power efficiency, low cost and reliability of SCLs make them very attractive for OPLL arrays.

A schematic diagram of a typical heterodyne OPLL is shown in Figure 5. The beat signal between a commercially available SCL and a narrow linewidth master laser is detected and amplified. An electronic mixer is used to down convert the beat signal using an RF

reference oscillator. The down-converted signal is then filtered, and fed back to the laser to close a negative feedback loop. In steady state, the frequency of the SCL satisfies [7]

$$\omega_s = \omega_m + \omega_{RF}, \tag{9}$$

where ω_s is the (angular) frequency of the SCL laser, ω_m and ω_{RF} are the frequency of the master lasers and the RF oscillator respectively. It should be noted that $\omega_s = \omega_m - \omega_{RF}$ is also a solution, but for simplicity the '+' sign was chosen. The phase of the SCL is also tracked and satisfies

$$\phi_s = \phi_m + \phi_{RF} + \phi_e \tag{10}$$

where ϕ_e is a a constant phase error necessary to maintain steady state. In the high loop gain regime ϕ_e is typically small and can be neglected (for a reasonably stable laser).

Small signal deviations about the steady state (noise) can be linearized and analyzed using standard control system analysis methods [7]. It can be shown that the phase noise of the SCL, within the bandwidth of the loop, tracks the phase noise of the master laser, while suppressing its own phase noise [5].

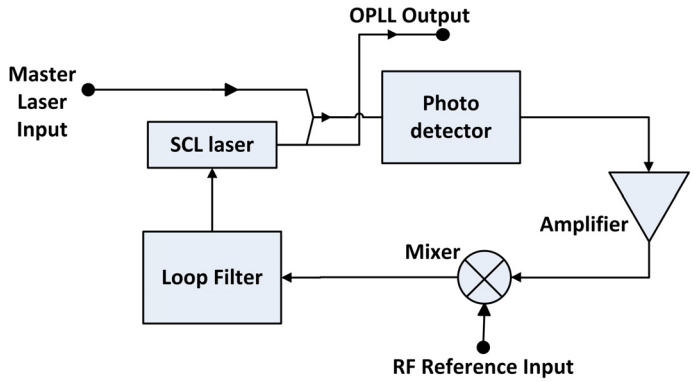

Figure 5. Schematic diagram of a typical heterodyne OPLL

One of the key requirements of an optical phased array is that all sources have exactly the same defined frequency. Referring to Figure 1 - provided all the OPLLs in the array are fed by the same master laser and RF oscillator, all the OPLLs outputs have the same frequency, as can be seen by Equation (9). The phase of the output field of the n^{th} OPLL is given by

$$\phi_{s,n} = \phi_m + \phi_{RF} + \phi_n + \phi_{e,n} \tag{11}$$

For high enough DC gain, the last term of Equation (11) can be neglected. By controlling the electronic phase shift ϕ_n we can obtain precise control over the phase of the array elements, which is required to obtain the desired beam steering.

From section II-C, an application for deep space communication would require the realization of (2D) array that contains about $(300)^2 \sim 100,000$ elements. This immediately implies that any such realization would have to be based on an on-chip fabrication of arrays of lasers together with at least some of the necessary electronics and

optoelectronic devices. Despite the fact that this is a true technological challenge, several groups have reported vertical-cavity surface-emitting laser (VCSEL) 2D laser arrays that can support tens to hundreds of laser elements per dimension and can achieve output powers of several hundred watts (but typically suffer from poor fill factors) [8, 9, 10]. There is an ongoing effort to fabricate integrated optoelectronic devices.

Since we are interested in precise control over the fringe pattern caused by interference of the array's elements, it is important to analyze the effect of the different sources of phase noise on the interference pattern. Phase noise, as manifested in the linewidth of the beam, causes a reduction of the visibility of the fringe pattern, and an unstable behavior of the main lobe position. The aim of the next section is to identify the statistical characteristics of these effects.

A. Performance of an OPLL-based phased array.

Though there are several sources of phase noise in the system, the most significant one by far is the residual phase noise due to the finite loop bandwidth. Therefore, other noise types, such as phase noise due to finite master laser linewidth, constant phase errors due to inaccuracies in the electronics, or due to slowly drifting frequencies are all neglected in the following analysis.

The phase locked loop has a finite bandwidth mainly due to the frequency modulation (FM) response of the laser and time delays in the loop. Outside the loop bandwidth the slave lasers are unable to track the master laser, and their own phase noise is not suppressed. The phase noise of each free running slave laser is uncorrelated with the others, and is mainly due to spontaneous emission. Following the analysis of [5] we will model the free running phase noise as a Gaussian process and treat the loop as a linear filter. Since the free running phase noise is assumed to be Gaussian, the linearly filtered phase noise would also be a Gaussian random process.

Next, consider the sum of Equation (2). Assuming equal power in each element of the array, and linear phase increment profile, we can express the term responsible for the fringe pattern as follows

$$I \sim \left| \mathcal{E}\left(\frac{2\pi d_s}{\lambda_0 L} x - \Delta\phi \right) \right|^2 = \left| \sum_{k=-M}^{M} e^{-ik(\frac{2\pi d_s x}{\lambda_0 L} - \triangle\phi) + i\phi_{n,k}(t)} \right|^2 \tag{12}$$

where $\phi_{n,k}(t)$ stands for the phase noise of the k^{th} emitter. We treat all $\phi_{n,k}(t)$ terms as a random process and the other variables as deterministic. We further assume that all phase noise terms (different ks) are uncorrelated (as they represent two independent free running lasers). Our goal is to calculate the expectation value and variance of the sum. At each time sample, the ensemble of sample functions is Gaussian distributed by assumption. Expanding Equation (12) and taking the expectation value we find that the average value of the field intensity is

$$\langle I(t)\rangle \sim (2M+1) + e^{-\sigma^2} \times \left\{ \sum_{\substack{\{j,k\}=-M \\ j\neq k}}^{M} e^{-i(k-j)(\frac{2\pi d_s x}{\lambda_0 L} - \triangle\phi)} \right\} \tag{13}$$

where σ^2 is the noise variance of $\phi_{n,k}(t)$.[3] To obtain an explicit expression, we assume that each beam has a Gaussian profile of width d_a as in section II, to yield

$$I(x,y,L) = \frac{P_0 d_a^2 \pi}{2\lambda_0^2 L^2} e^{-\frac{1}{2}\left(\frac{\pi d_a}{\lambda_0 L}\right)^2 (x^2+y^2)} \times \left\{ (2M+1)(1-e^{-\sigma^2}) + e^{-\sigma^2} \frac{\sin^2\left(\frac{\pi d_s}{\lambda_0 L}(2M+1)[x - \frac{\Delta\phi\lambda_0 L}{2\pi d_s}]\right)}{\sin^2\left(\frac{\pi d_s}{\lambda_0 L}[x - \frac{\Delta\phi\lambda_0 L}{2\pi d_s}]\right)} \right\} \tag{14}$$

The visibility, $V = \frac{I_{max}-I_{min}}{I_{max}+I_{min}}$, can be calculated by evaluating the maximum and minimum points in proximity of the main lobe. A plot of visibility as a function of σ is given in Figure 6.

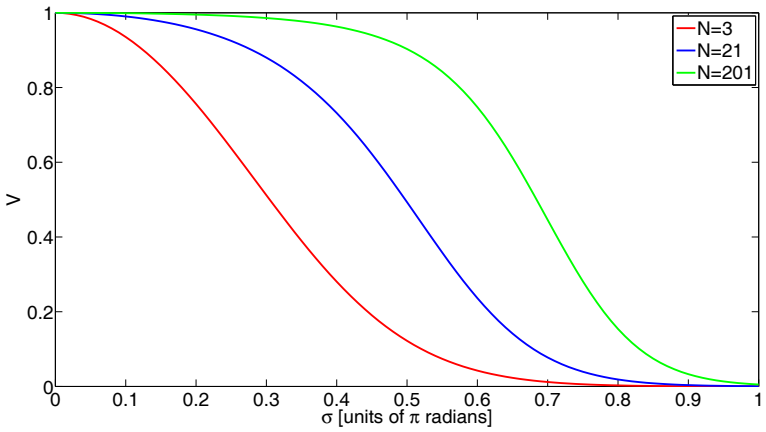

Figure 6. Visibility vs. residual phase noise for different N = (2M+1) values

To get more insight out of that equation, assume $(2M+1) \gg \frac{2\pi}{\triangle\phi}$ (large array) and $\sigma \ll 1$ (true in stable PLLs), and compute the visibility V

$$V(M \gg \frac{2\pi}{\triangle\phi},\ \sigma \ll 1) \approx \frac{(1-\sigma^2)(2M+1)^2}{(1-\sigma^2)(2M+1)^2 + 2\sigma^2(2M+1)} \tag{15}$$

Notice that as $M \to \infty$, the visibility goes to 1. Hence, *by implementing a large number of emitters in the array, we can mitigate the effect of untracked residual phase noise.*

It should be noted that if the assumption on Gaussian zero mean noise could also be made for constant phase errors due to electronic inaccuracies, or due to slowly varying frequency

[3] We have assumed that all $\phi_{n,k}(t)$ are independent and identically distributed Gaussian random variables, with variance σ^2.

drift, the result of this section could be applied to them as well. However, If the different sources are somehow coupled (for example, thermal fluctuation effect all OPLLs in the same way), these constant errors are no longer uncorrelated, and the effects of this systematic error should be re-analyzed.

IV. Experiment

Using the technique discussed above, beam steering was demonstrated in a proof-of-principle experimental array consisting of two OPLLs.

A. Setup

The experimental setup is similar to the one of Figure 1 with N = 2. Two commercially available "slave" distributed feedback (DFB) SCLs at a wavelength of 1539 nm were phase-locked to an ultra narrow linewidth "master" fiber laser using a heterodyne OPLL configuration. A small fraction of the output from each laser was split off for use in the OPLL, while the remaining fraction constituted the observed output into the imaging system. An RF signal at 1.7 GHz was split into two and input to each OPLL. One of the RF branches had a controllable phase shifter, which was used to shift the phase by up to π radians at that frequency. The OPLLs were similar to Figure 5 with the loop filter being a passive lag filter.

To achieve a high fill factor the output of each OPLL was connected to the input of a custom made fiber holder array. By choosing suitable outputs, the spacing between emitters was

$$d_s = b \times n, \qquad n = 1, 2...7 \tag{16}$$

where $b = 250\mu$m and n could be varied from 1 to 7. The diverging beams from the fiber array were collimated using a custom micro lens array. The far field pattern was then imaged using a camera at distance $z = 431.8$ mm from the lens array plane. A schematic of the optical system is shown in Figure 7.

The micro fiber holder array could support up to eight laser inputs. In our setup the eight different inputs of the array were used to image far field pattern with different fill factors, with the distance between sources changed as described by Equation (16).

B. Experimental Results

The RF phase shifter was first characterized, verifying that at the operating frequency of 1.7 GHz a phase shift of π radians could be obtained. The two lasers were simultaneously phase-locked to the master laser and characterized by measuring the beat signal between the master and slave lasers using an electronic spectrum analyzer (SA). Figure 8 shows the output of the SA for one of the OPLLs (the second OPLL had a very similar beat signal spectrum, and is therefore not shown).

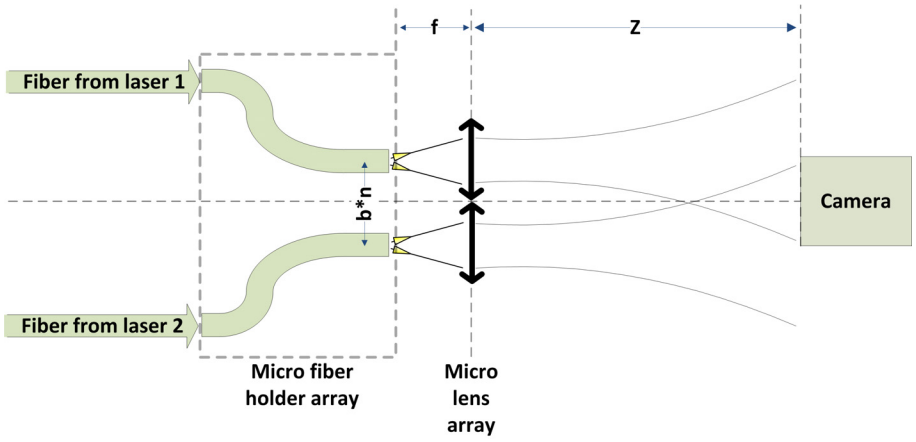

Figure 7. The optical imaging system.

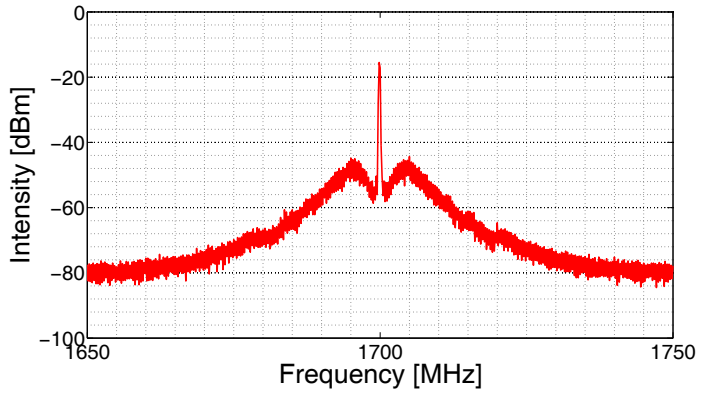

Figure 8. Spectrum of the master-slave beat signal during phase-lock for one of the two heterodyne OPLLs. The residual phase error in the loop is about 0.4 rad. The resolution bandwidth is 100 kHz.

The two lasers were locked to the master laser simultaneously to obtain a fringe pattern. Figure 9 shows the affect of simultaneous lock of the two lasers.

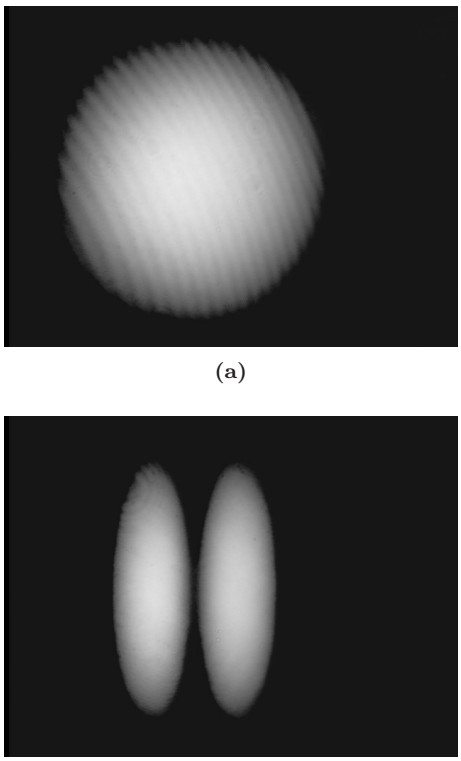

(a)

(b)

Figure 9. Image of the the far field on the camera for $n = 1$. (a) The lasers are out of lock (fringes are due to aperture). (b) The two lasers are simultaneously locked and a fringe pattern becomes visible.

As seen in Figure 10, a change in the RF phase by π causes a fringe shift by one half of the fringe separation, demonstrating direct *electronic* control over the optical phase, *on a one-to-one basis*. From Figure 10(b), the fringe visibility is not optimal, and the minima do not go down to zero. Besides poor camera dynamic range, the main factors that reduce the visibility are mismatched optical intensities, mismatched polarization states of the lasers, and residual phase errors in the OPLL's that significantly reduce the visibility. Improving the loop bandwidth, matching laser intensities and polarization states should significantly improve fringe visibility.

The width of the Gaussian beam, the beam separation, and the distance to the camera z were used to calculate the theoretical fringe pattern using Equation (5). This fringe pattern is plotted along with the experimental measurement in Figure 11, showing excellent agreement.

The experiment described above was performed with different values of the separation between sources. The fiber holder array structure allowed us to change the separation according to Equation (16). Representative measured fringe patterns for $n = 1$ and $n = 2$ are shown in Figure 10 (a) and (b) respectively. As the separation is increased

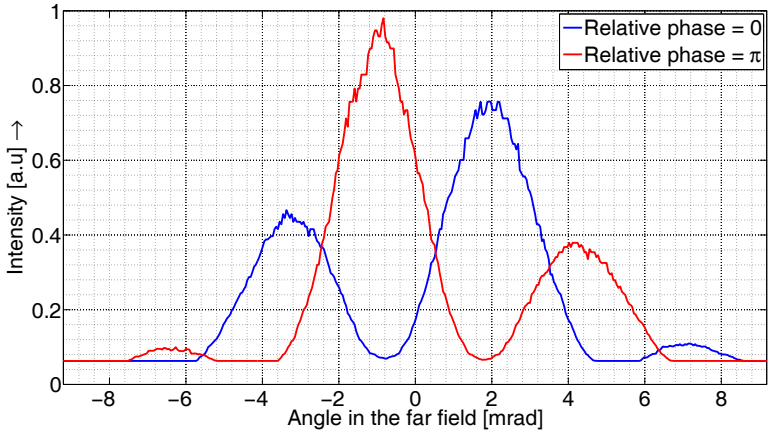

(a)

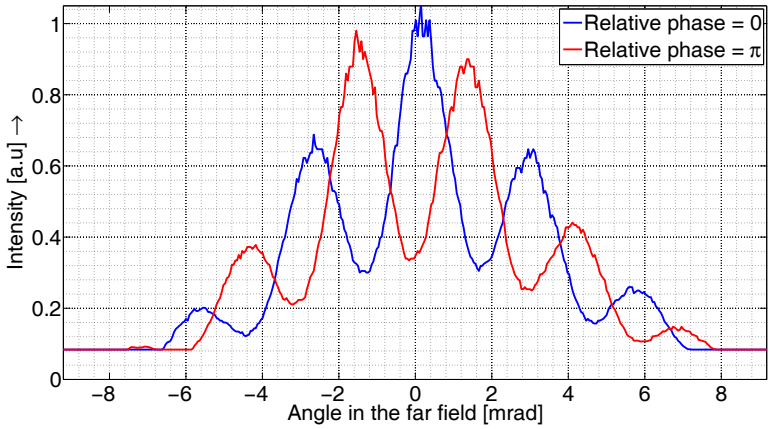

(b)

Figure 10. Horizontal section of the measured intensity with (a) $n = 1$, $\gamma \approx 0.7$ (b) $n = 2$, $\gamma \approx 0.35$, for RF phase shifts of 0 and π, demonstrating electronic beam steering.

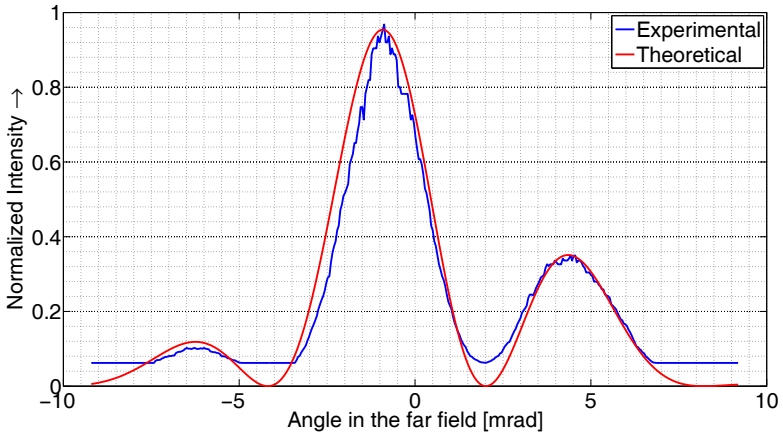

Figure 11. Comparison of the experimental fringe pattern with the theoretical calculation ($n = 1$).

(corresponding to lower fill factors, γ), the number of fringes within the envelope increases, accompanied by a decrease in the angular width of the central lobe.

The average separation between the fringes was extracted from the graphs and plotted as a function of the inverse source separation $1/d_s$, as shown in Figure 12, and agreed well with the theoretical prediction (Equation (5)) for the change in fringe separation with spot separation.

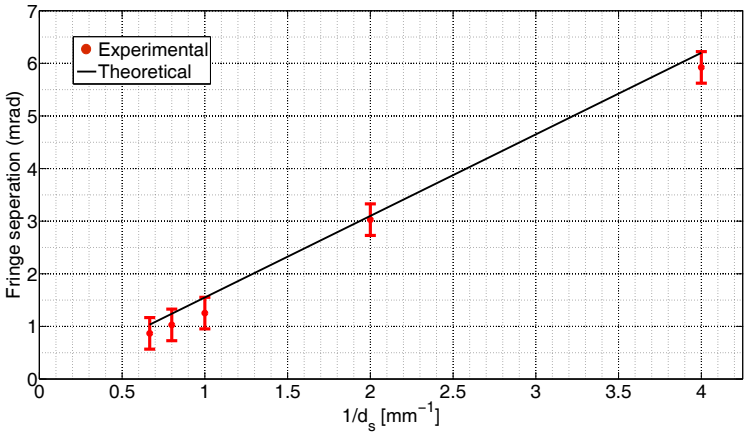

Figure 12. Separation between fringes as a function of the inverse beam separation $1/d_s$, compared to theory.

V. Conclusion and Discussion

A possible paradigm shift in deep-space optical communications, using an optical phase lock loop based phased array was analyzed and a two-laser array was experimentally demonstrated and compared to theory. Realization of a large element array would enable communication architectures that utilize constant-envelope modulations, such as binary phase-shift keying (BPSK) or offset quadrature phase-shift keying (O-QPSK), that would allow future optical communications terminals to use very high efficiency laser diodes ($>$ 70 %). An optical phased array exercising precise control over the phase of the transmitted beam permits the use of such modulation schemes while maintaining the potential to emit hundreds of watts of power, in addition to offering a high degree of redundancy in transmitter power and steering capability from the multiplicity of array elements. When coupled with quantum-limited optical receivers that enable communication at a photon efficiency that far exceeds the state-of-the-art coherent detection schemes (i.e., heterodyne or homodyne) [11], we can envision future deep-space optical transmitters, operating at efficiencies greater than 70 %, weighing on the order of 10 kg, while providing steerable optical output power exceeding 100 watts. This efficiency is nearly an order of magnitude higher than current optical communications terminals, and even higher than state-of-the-art RF communication terminals.

It was demonstrated both experimentally and theoretically that the performance of the

optical phased array is highly dependent on the fill factor γ. It is therefore desirable to increase the fill factor as much as possible. Furthermore, for any realistic array, the number of elements for each dimension needs to be in the hundreds. Therefore the primary technical future challenges are increasing the total number of elements in the transmitter arrays and improving the fill factor, in addition to enabling high-efficiency coherent modulation of the array elements for communication. These require on-chip integration of the array elements and the supporting electronics in a scalable architecture. The fully-electronic phase-control technology we have demonstrated in this article offers a novel solution that is well-suited to respond to these needs.

In the experiments described in this article, we have demonstrated fringe steering using OPLL based electronically controlled optical phased arrays. The fringe pattern was compared to the theoretical pattern and good agreement between the two was obtained. The lasers were demonstrated to simultaneously remain locked for periods exceeding 30 minutes. This could be improved by using modified loops and/or SCLs that would enable stable phase locking with higher gain. When implemented in a multi-element array, we expect that the effect of an occasional loss of lock in a single element would be negligible. The fringe pattern was stable, and any instability was attributed to changes in length of the optical fibers (fiber breathing) due to environmental changes. It is expected that an integrated phased array with no fibers will be much more stable.

References

[1] J. Katz, S. Margalit, and A. Yariv. Diffraction coupled phase-locked semiconductor laser array. *Applied Physics Letters*, 42(7):554–556, 1983.

[2] D. P. Resler, D. S. Hobbs, R. C. Sharp, L. J. Friedman, and T. A. Dorschner. High-efficiency liquid-crystal optical phased-array. *Optics Letters*, 21:689–691, 1996.

[3] N. Satyan, W. Liang, A. Kewitsch, G. Rakuljic, and A. Yariv. Coherent power combination of semiconductor lasers using optical phase-lock loops. *IEEE Journal of Selected Topics in Quantum Electronics*, 12:240–247, 2009.

[4] A. Yariv. Dynamic analysis of the semiconductor laser as a current-controlled oscillator in the optical phased-lock loop: applications. *Optics Letters*, 30:2191–2193, 2005.

[5] N. Satyan, W. Liang, and A. Yariv. Coherence cloning using semiconductor laser optical phase-lock loops. *IEEE Journal Of Quantum Electronics*, 45:755–761, 2009.

[6] C. H. Henry, R. A. Rogan, K. A. Bertness. Spectral dependence of the change in refractive index due to carrier injection in GaAs lasers. *J. Appl. Phys.*, 52:4457-4461, 1981.

[7] F. M. Gardner. *Phaselock techniques*. Wiley-Interscience, Hoboken, N.J., 2005.

[8] C.L. Chua, R.L. Thornton, D.W. Treat, and R.M. Donaldson. Independently addressable vcsel arrays on 3μm pitch. *IEEE Photonics Technology Letters*, 10(7):917 –919, 1998.

[9] H. Chen, D. Francis, T. Nguyen, W. Yuem, G. Li, and C. Chang-Hasnian. Collimating diode laser beams from a large-area vcsel-array using microlens array. *IEEE Photonics Technology Letters*, 11(5):506 –508, 1999.

[10] M. Grabherr, M. Miller, R. Jger, D. Wiedenmann, and R. King. Commercial vcsels reach 0.1 wcw output power. *Proc. SPIE*, 5364:174–182, 2004.

[11] B. I. Erkmen, B. E. Moision, and K. M. Birnbaum. A review of the information capacity of single-mode free-space optical communication. *Proc. SPIE*, 7587:75870N, 2010.